The Dynamical Structure of the Kuiper Belt

Martin J. Duncan

Department of Physics, Queen's University
Kingston, Ontario, Canada K7L 3N6

Harold F. Levison

Space Science Department
Southwest Research Institute, Boulder, CO 80302
and

Stuart Mark Budd

Department of Physics, Queen's University
Kingston, Ontario, Canada K7L 3N6

Running Title: *Kuiper Belt Structure*

Martin J. Duncan
Physics Department
Queen's University
Kingston, Ontario K7L 3N6
Canada
(613) 545-2716, Fax: (613) 545-6463
duncan@astro.queensu.ca

ABSTRACT

Results are presented of integrations of a representative sample of thousands of test bodies in the Kuiper belt for times up to the the age of the solar system. Using this survey, the main regions of dynamical stability (and instability) are mapped out as a function of the particles' semi-major axes, eccentricities and inclinations. Much of the dynamical structure is shown to be correlated with mean motion and secular resonances. Weak dynamical instabilities are confirmed to be capable of producing an influx of Neptune-approaching bodies even on Gyr timescales. The integrations are also compared with current observations of bodies in this region. Implications for the early evolution of the Kuiper belt, its current structure, and the origins of short period comets are discussed.

1. INTRODUCTION

The trans-Neptunian region of the solar system has become the focus of considerable interest, mainly due to the detection of dozens of 100 km – sized bodies beyond Neptune's orbit (see Jewitt & Luu 1995). This set of discoveries has substantiated arguments dating back over 40 years that the disk of planetesimals that formed the planets should extend past Neptune (Edgeworth 1949, Kuiper 1951). This hitherto hypothetical trans-Neptunian disk is currently called the Kuiper belt.

The search for objects in the Kuiper belt was prompted in part by the suggestion that the Kuiper belt is the source of short-period comets. Fernandez (1980) first suggested that such a belt of distant icy planetesimals could serve as the source of the short-period comets and would be more dynamically efficient than evolving long-period comets inward as first suggested by Newton (1893; see also Everhart 1972, 1977). Duncan *et al.* (1988) strengthened this argument by performing dynamical simulations which showed that a cometary source with a low initial inclination distribution was far more consistent with the observed orbits of the short period comets than the randomly distributed inclinations of comets in the Oort cloud (see also Quinn et al. 1990). Arguments associating the Kuiper belt with the origin of short-period comets have been dramatically bolstered by the detection of a population of $\sim 2 \times 10^8$ bodies of radii ~ 10 km in a highly flattened distribution in this region (Cochran et al. 1995).

Duncan et al. (1988) and Quinn et al. (1990) left as an unsolved issue the process of the evolution of objects from low-eccentricity orbits in the Kuiper belt to planet crossing orbits. Torbett (1989) performed direct numerical integration of test particles in this region including the perturbative effects of the four giant planets, although the planets were taken to be on fixed Keplerian orbits. He found evidence for chaotic motion with an inverse Lyapunov exponent (i.e. timescale for divergence of initially adjacent orbits) on the order of Myrs for moderately eccentric, moderately inclined orbits with perihelia between 30 and 45 AU. Torbett & Smoluchowski (1990) extended this work and suggested that even particles with initial eccentricities as low as 0.02 are typically on chaotic trajectories if their semi-major axes are less than 45 AU. Except in a few cases, however, the authors were unable to follow the orbits long enough to establish whether or not most chaotic trajectories in this group led to Neptune–crossing.

Since the initial work by Torbett, several authors have performed simulations involving longer times and larger numbers of particles. Gladman & Duncan (1990) performed a 2×10^7 year integration of a small number of particles initially on circular orbits between 30 and $40\,AU$. Levison & Duncan (1993) and Holman & Wisdom (1993) performed more extended integrations, for 10^9 and 2×10^8 years, respectively. In both papers, the authors studied the behavior of objects initially on low-inclination, nearly-circular orbits inside of $45 AU$. Both groups found that indeed the belt was dynamically sculpted on million to billion year timescales, thereby potentially providing a continuing supply of short-period comets. It was noted by these researchers that particularly stable (or unstable) bands were associated with mean motion and/or secular resonances, but these correlations were not investigated further. As we were writing this paper, we received a preprint from Morbidelli, Thomas, & Moons (1995) which presented the results of an approximate analytic study of the resonant structure of the Kuiper belt. This paper provides a theoretical understanding of the behavior seen near the mean motion resonances in the early numerical studies.

The purpose of this paper is to extend our earlier numerical investigations for times up to the age of the solar system and for a wider range of orbital elements – in particular to study orbits of higher eccentricities and inclinations. This investigation has three goals: *i*) to map out better the current dynamical structure of the trans–Neptunian region and to relate its main features to mean motion and secular resonances where possible, *ii*) to determine which regions of the Kuiper belt are currently unstable and thus may be supplying the Jupiter-family comets that we see today, and *iii*) to combine the results of these integrations with some simple assumptions concerning the original distribution of residual planetesimals in order to build rough models of the current density distribution in the Kuiper belt.

In Section 2 of the paper we describe how the simulations were performed and give the basic results. In Section 3, we discuss billion year integrations of some of the observed 100-km bodies in the Kuiper belt and discuss the theoretical implications of these calculations. In Section 4 we use the simulations in Section 2 to estimate the current number of objects in the Kuiper belt as well as their surface density distribution. A summary of our conclusions is presented in Section 5.

2. RESULTS OF THE SIMULATIONS

In order to develop a complete understanding of the behavior of objects in the Kuiper belt, it is necessary to cover as wide a range in orbital element space as possible while integrating the orbits for as long as possible. The ability to integrate for the age of solar system the orbits of objects in all regions of orbital0 element space at the resolution necessary to discover all of the Kuiper belt structure is still beyond the reach of modern facilities. Thus, the numerical integrations we performed were divided into 2 sets. In the first, our intent was to achieve reasonably high resolution in semi-major axis ($\Delta a = 0.05\,AU$) and to integrate for the age of the solar system ($\tau = 4 \times 10^9$ yr). In this set we restricted ourselves to the study of 1300 low-inclination orbits ($i = 1°$) at six values of the eccentricity (0.01, 0.05, 0.1, 0.15, 0.2, and 0.3). In the second set, we reduced the spatial and temporal coverage (choosing $\Delta a = 0.1\,AU$ and $\tau = 10^9$ yr) to study the behavior for a wider range of inclinations. Thus, we integrated the orbits of 3000 test particles at three values of eccentricity (0.01, 0.05, and 0.1) and 8 values of inclination (5°, 10°, 15°, 20°, 30°, 45°, 60°, and 90°). For each particle in a run, the initial longitude of perihelion, the longitude of the ascending node and the mean anomaly were chosen randomly from a uniform distribution between 0 and 2π.

The numerical integrations were performed using our general purpose solar system integration package named Swift (Levison & Duncan 1994). The integrator that we used is based on the highly efficient symplectic algorithms introduced by Wisdom & Holman (1991). In some of the simulations described below, we incorporated individual timesteps for the test particles using the approach of Saha & Tremaine (1993). In cases where this was done, we carefully compared the results from the modified code against one using fixed timesteps and verified that the results agreed within the statistical uncertainties inherent in dealing with chaotic systems.

Our experience with several initial test runs suggested that particles with pericenters (q) less than $32\,AU$ were greatly perturbed and thus were unstable. As a result, in the first few runs, particles were integrated until either they i) had $q < 32\,AU$, ii) had apocenters beyond a radius on the order of $100\,AU$ or iii) the integration time exceeded the duration τ of the simulation. With the discovery of several 100-km Kuiper belt objects that are currently near $32\,AU$, it became obvious (Marsden 1994) that the protection against Neptune encounters offered by mean motion resonances (notably the 2:3 resonance) was critical to the understanding of the stability of at least some objects in the Kuiper belt. Therefore, in the later runs we integrated particles until either they i) came within a Hill radius of a planet, ii) had pericenters interior to 25 AU, iii) had apocenters beyond a radius on the order of $100\,AU$ or iv) survived for the entire duration, τ, of the simulation. Since several CPU months of computer time were expended on the early runs, we did not re-run them. However, we inspected the data in these runs to ensure that no particles which were protected from a Neptune encounter were erroneously removed simply because they crossed $32\,AU$.

The key results of our 4 billion year and 1 billion year integrations are shown in Figures 1 and 2, respectively. The colored strips indicate the dynamical lifetime (as described in the last paragraph) of a particle as a function of two of its initial orbital elements; a and e in Figure 1 and a and i in Figure 2. Strips that are colored yellow represent objects that survived for the length of the integration; 4 billion years in Figure 1 and 1 billion years in Figure 2. Objects that were stable for the length of the integrations typically had semi-major axes which remained nearly constant, while some of their eccentricities and inclinations varied. However, there was no secular growth observed in these quantities. Not surprisingly, these variations were more pronounced near the mean motion resonances with Neptune (shown in Figure 1) than at large heliocentric distances.

The dark regions show orbital elements that were very unstable. The regions were depopulated at early epochs and thus are not the source of the Jupiter-families comets that we see today. The regions colored orange in Figure 1 are regions in which objects remained stable for billions of years and then went unstable and suffered a close encounter with Neptune. These regions are potential sources of the Jupiter-family comets, as we discuss later.

As can be seen from the Figures 1 and 2, the Kuiper belt has a complex structure, although the general trends are easily described. In general, objects with perihelion distances, q, less than $\sim 35AU$ (shown as a red curve in Figure 1) are unstable. Presumably, this is due to the cumulative effects of random forces due to Neptune exerted near perihelion.

The main exceptions to the trend toward instability at small perihelion distances are the low-inclination orbits librating in low-order Neptune mean motion resonances. This is illustrated in Figure 1, where we have plotted the location of the most important of these resonances. The banded structure near the resonances is due to that fact that we did not deliberately place objects in the resonance and their critical arguments were chosen at random. Thus, some particles near the resonances were initially librating while others were circulating.

Notice that for orbits with $e \gtrsim 0.1$ and $a < 42\,AU$ the only stable orbits are those in these resonances. To first order, the stability of these orbits at low-inclination can be understood on theoretical grounds due to the work of Morbidelli, Thomas, & Moons (1995). They showed that, in contrast to the Kirkwood gaps in the asteroid belt, this stability is due to the absence of secular resonances embedded in the mean motion resonances. However, we have found that many of the low order mean motion resonances are unstable for inclinations greater than about $25°$, as can be seen in Figure 2. To emphasize this point, in Figure 3 we have reproduced the bottom panel of Figure 2 (with a different color table for enhanced visibility) and have indicated by green lines the locations of the dominant mean motion resonances with Neptune. This instability might be associated with secular resonances discussed next.

The last unexplained features in the first two figures are two bands within which particles become unstable on a 10^7 year timescale: one between $\sim 40\,AU$ and $\sim 42\,AU$ at low inclinations, and one at $i \sim 15°$ between $\sim 36\,AU$ and $\sim 39\,AU$. These bands are associated with secular resonances with Uranus and Neptune. This can be seen in Figure 3, which shows the results of our 1 billion year integration. These particles all had initial eccentricities of 0.01. Also shown are the locations of the Neptunian longitude of perihelion secular resonances (ν_8, in red) the Neptunian longitude of the ascending node secular resonances (ν_{18}, in yellow) as determined by Knežević *et al.* (1991). It is important to note that a significant fraction of the clearing of the Kuiper belt occurs where these two resonances overlap. This includes the low inclination regions near $36\,AU$ and between 40 and $42\,AU$, as seen in Figure 1. The behavior of particles in these regions is typical of what is expected for secular resonances — a secular growth in eccentricity and/or inclination.

As we mentioned above, the low order Neptune mean motion resonances are unstable for high inclinations. It can be seen in Figure 3 that the secular resonances associated with the longitude of perihelion as calculated by Knežević *et at.* (1991) converge on the 3:4 and 2:3 mean motion resonances for large inclinations (although as they pointed out, their theory may have difficulties very near the mean motion resonances and at inclination above $\sim 30°$). This suggests that the instabilities seen near these resonances are caused by the overlap of the secular and mean motion resonances.

In order to test the hypothesis of resonance overlap, we carefully examined the orbits of a few particles near the 3:4 mean motion resonance with initial $i = 45°$ and $e = 0.01$ (seen in Figure 3). We found that some of these particles librated about the mean motion resonances while others librated about the secular one. This confirmed the close proximity of the two resonances in this region of phase space. We found that the particles between these resonances appear to be chaotic. The behavior of such a particle is shown in Figure 4. Figure 4a shows the temporal variation of critical argument of the ν_8 resonance (i.e. $\tilde{\omega} - \tilde{\omega}_{Neptune}$). At early times it appears that the particle was librating about the ν_8 resonance with a period of about 10^7 years. As its eccentricity was driven up (Figure 4c), the particle began to librate about the 3:4 mean motion resonance (Figure 4b). At late times, the object stopped librating about the ν_8. This behavior is reminiscent of the behavior of test particles near the ν_8 resonances at $i \sim 0$ and $a \sim 40\,AU$ (Levison & Stern 1995). Surprisingly, the particle in Figure 4 was a Neptune-crosser for most of the integration and yet it encountered Uranus before it encountered Neptune.

In addition to the instability associated with the 3:4 and the 2:3 resonances, we found that the 5:7 and 3:5 resonances are also unstable for large inclinations (see Figure 3). However, unlike the former two resonances, the results of Knežević *et at.* (1991) did not predict a nearby first order secular resonance for the 5:7 and 3:5 resonances. A careful examination of unstable orbits near the 5:7 resonance showed sporadic libration about this mean motion resonance and a secular increase in eccentricity, but no libration about the ν_7, ν_8, ν_{17}, or ν_{18} resonances. However, we found that at times when the eccentricity was large, the argument of perihelion was librating about 0 degrees, the inclination and eccentricity were anti-correlated, and the particle avoided Neptune. This behavior is typical of the Kozai mechanism (Kozai 1962, Thomas & Morbidelli 1995), although it is not the mechanism which initially drives up the eccentricity. Thus the exact mechanism for the instability remains unclear, but we believe that some type of secular resonance is the culprit.

In sum, we have established that mean motion resonances are typically stable at low inclinations, but typically unstable above $i \sim 25°$. However, we also found that there is a long-term leakage from the mean motion resonances even at low inclinations. For example, in Figure 5 we plot the dynamical lifetime of test particles in our 4 billion year integration with initial $e = 0.2$ and $i = 1°$ as a function of initial libration amplitude of the 2:3 mean motion resonance with Neptune, A_δ. Symbols on the dotted horizontal lines survived for the length of the integration. Those below the line became unstable and came within the Hill sphere of Neptune. Particles with initial $A_\delta \gtrsim 130°$ are unstable on short timescales, $\lesssim 10^8$ years. More importantly, objects with $70° \lesssim A_\delta \lesssim 130°$ are unstable on billion year timescales. Similar results were found for objects with orbits like that of Pluto (Levison & Stern 1995).

Long-term instabilities can be seen in other mean motion resonances. The behavior of a typical particle that leaves the 3:4 resonance at late times is shown in Figure 6. This particle began with $i = 1°$ and $e = 0.15$. The object was well within the resonance for most of the integration, although the libration amplitude seemed to vary chaotically. During this time the eccentricity (or perihelion distance) remained approximately constant. At roughly 3.3 billion years, the particle started to circulate about the mean motion resonance, the inclination grew to $\sim 20°$, and the object quickly encountered Neptune. It is important to note that this object initially had a perihelion distance very close to Neptune's orbit and thus it was protected by the mean motion resonance for billions of years, yet eventually became unstable.

2.1 The Source of Jupiter-Family Comets

One important aspect of the Kuiper belt is that it is the likely reservoir of the Jupiter-family comets. Therefore, we are interested in determining which regions of the Kuiper belt are currently supplying comets into Neptune-approaching orbits. In addition, since the main argument in favor of the Kuiper belt being the source of the Jupiter-family comets is the low inclination distribution of these comets, we are also interested in the inclination distribution of objects as they leave the Kuiper belt. Thus in Figure 7, we plot the inclination of objects as they left the Kuiper belt after a billion years as a function of their initial semi-major axes. The different symbols represent different initial eccentricities. Members of this population with initial $e \lesssim 0.1$ arise in a region between 34 and 42 AU and typically have inclinations less than 10 degrees as they leave the belt. A small fraction, which can have inclinations as high as 15 degrees, seem to be those leaking from the 2:3 resonance. Members of this population with initial eccentricities between 0.1 and 0.2 (shown as filled symbols in Figure 7) typically originate from two regions – a band between 42 and 50 AU and a zone inside of 40 AU of narrow bands centered on the low order mean motion resonances. Objects originating in the outer region have final inclinations $\lesssim 10°$. Objects originating in the zone inside of 40 AU with $e > 0.1$ can have surprisingly large inclinations – as large as 25°. We are presently unable to explain why these particles are forced to such high inclinations. It is interesting to note that there is a probable object (1995 GJ) in the Kuiper belt with an inclination of about 23°, although it is not currently thought to be in a mean motion resonance; with only a 1-day observed arc it is by no means clear that this *is* a Kuiper belt object.

In all of the simulations we have performed, we have found that at late times the flux of objects into Neptune-encountering orbits is fairly well approximated by a power law in time with an exponent of ~ -1. This is consistent with the results of the 200 million year integrations of Holman & Wisdom (1993). The exact exponent in the decay law is clearly dependent on the distribution of orbits left after the completion of planet formation. For example, Malhotra (1995) has argued that under some models of planet formation, Neptune would form closer to the Sun than its present location and that Neptune's outward migration would sweep up the vast majority of remaining particles in the inner regions of the Kuiper belt into low order mean motion resonances. However, we have seen that long-term erosion of particles with moderate libration amplitude can occur near these resonances as well. So, in most reasonable cases, the erosion is rather gradual and therefore must be continuing at the current epoch.

3. ORBITAL STABILITY OF KNOWN KUIPER BELT OBJECTS

As of the writing of the paper, there are 24 objects with radii of about 100 km that are reasonable candidates for membership in the Kuiper belt. For 17 of these, noncircular orbits have been published by Brian Marsden in the "Minor Planet Circulars" and "Minor Planet Electronic Circulars". Marsden requested that we integrate these orbits to determine their stability. In this section, we present the results of these integrations and compare them with the results of the simulations presented in the last section.

A list of the orbits we integrated is presented in Table 1. Column 1 of the table lists the name of each object. A parenthetical dagger symbol (†) after the name means that planetary perturbations were not considered in the computation of the orbit since the observed arc was so small. Note that for several objects we integrated more than one orbit. The objects with multiple orbits are those that Marsden placed in mean motion resonances with Neptune on the grounds that they are currently too close to the Sun to be stable unless they are in such a resonance. However, observations of these objects were often insufficient to constrain which resonance they actually occupied. In some cases Marsden used the results of these integrations in selecting which orbits to list in the MPEC. In all, we integrated 32 orbits for up to 1 billion years each. The particles were integrated until either they i) came within a Hill radius of a planet, ii) had apocenters beyond a radius of 150 AU or iii) the integration time exceeded the duration of the simulation.

Column 2 lists the semi-major axis, while Column 3 indicates which Neptune mean motion resonance the object occupies (if any). Columns 4–8 list the remaining orbital elements: eccentricity (e), inclination (i), argument of perihelion (ω), longitude of the ascending node (Ω), and mean anomaly (M) at the epoch 1995 March 24, respectively. The last column indicates the status of the orbit. A reference to an MPC issue implies that the orbit was stable and is the current best orbit for this object. A status of 'Stable' implies that the object survived to the end of our integration but the orbit was not adopted by Marsden.

The current semi-major axes and eccentricities of all 32 orbits listed in Table 1 are also plotted as circles in Figure 1. Note that although the simulation data only includes objects with $i = 1°$, all the tabulated orbits were plotted, independent of their inclinations. The filled green circles indicate the orbits accepted by Marsden. The open green and red circles represent the other stable and unstable orbits, respectively. The filled blue circles show the current heliocentric distances of the remaining 7 Kuiper belt candidates for which only circular orbits have been computed.

The main result of a comparison between the simulations presented in the last section and the Marsden's orbits is that objects inside of $\sim 42\,AU$ have sufficiently high eccentricities that they must be in Neptune mean motion resonances to be stable. Objects outside of this region appear to have lower eccentricities and are not in obvious mean motion resonances. It is interesting to note that this transition occurs near the location of the ν_8 secular resonances.

At first sight, it is surprising that there are, as yet, no known objects with semi-major axes between 36 and 39 AU, despite the fact that our simulations indicate that most objects in this region are stable provided their eccentricities are less than $\lesssim 0.05$. (It is interesting that a similar region exists in the outer asteroid belt; Duncan 1995.) If the 36 – 39 AU region is indeed not populated, then some mechanism other than the long-term gravitational effects of the planets in their current configuration must have cleared it. Two main mechanisms that may have accomplished this come to mind:

- The hypothetical early outward migration of Neptune would cause its mean motion resonances to sweep through this region thereby sweeping most objects into its mean motion resonances (Malhotra 1995). This mechanism was first proposed to explain Pluto's current orbit (Malhotra 1993). One possible problem with this mechanism is that in order to get Pluto into its current orbit, Neptune must have had an initial semi-major axis of $25\,AU$. Thus, the initial location of the 1:2 mean motion resonance ($40\,AU$) would have been inside the location of all the known Kuiper belt objects that are not in mean motion resonances (roughly half of the total number). In the context of this mechanism, it is difficult to understand why most of these objects were not captured into the 1:2 resonance as Neptune migrated to its current location. In general, this mechanism predicts that the mean motion resonances would be over-populated relative to a more uniform initial distribution.
- Some process may have pumped up the eccentricity and inclinations of particles in this region above $e \sim 0.05$ and/or $i \sim 10^\circ$ where the dynamical lifetimes are short. One method for exciting random motion in a disk is by mutual gravitational encounters between objects in the disk. In this vein, it is interesting to note that the escape velocity of the largest known Kuiper belt object is approximately $200\,m/s$ which is about 5% of its heliocentric orbital velocity. Thus, if there were initially enough of these objects for the Kuiper belt to be dynamically relaxed by mutual gravitational scattering, then they would have a typical eccentricity of a few percent, not quite enough to depopulate the region of interest. However, there are other mechanisms that could produce higher eccentricities. If the Kuiper belt initially had objects the size of Charon ($\sim 500\,km$), then the typical eccentricity would be $\gtrsim 0.1$. Indeed, there is some observational evidence for such a population (Stern 1991). In addition, the eccentricities of some of the objects may have been pumped up due to the gravitational perturbations of the giant planets. These in turn could have excited the rest of the population through mutual encounters (cf. Wetherill 1991). In either case the region of interest may have been depopulated, except in the resonances where large eccentricity orbits are stable. Unlike the previous hypothesis, this mechanism predicts that the mean motion resonances would *not* be over-populated relative to a more uniform initial distribution.

These two explanations are not exhaustive. Physical collisions and gas drag may have played an important role (Stern 1995). Nonetheless, these two models make very different predictions about the distribution of objects in the Kuiper belt. Thus it seems likely that further observations will help resolve which mechanism was dominant.

4. ESTIMATES OF THE NUMBER OF KUIPER BELT OBJECTS

It is possible to combine the results of the simulations presented in Section 2 with the total number of Jupiter-family comets to estimate the total number of comet-sized objects in the Kuiper belt. The total number of Jupiter-family comets (both active and extinct) can simply be expressed as

$$N_{JFC} = N_{KB}\ r_{Nx}\ f_{JFC}\ L_{JFC}, \tag{1}$$

where N_{KB} is the current number of comets in the Kuiper belt, r_{Nx} is the fraction of particles that leave the Kuiper belt per year, f_{JFC} is the fraction of particles that become Jupiter-family comets once they leave the Kuiper belt, and L_{JFC} is the dynamical lifetime of a Jupiter-family comet. Recent simulations, including those in Section 2, now allow us to estimate all of the parameters:

L_{JFC}: By direct numerical integrations, Levison & Duncan (1994) showed that the median dynamical lifetime of the Jupiter-family is 3.3×10^5 years.

f_{JFC}: From their numerical integrations, Duncan, Quinn, & Tremaine (1988) found that $f_{JFC} = 0.17$. However, in a set of more accurate simulations currently in progress, we have integrated a large fraction of the particles shown in Figure 7 until they were either ejected from the solar system or became visible Jupiter-family comets. We found that $f_{JFC} = 0.34$ and adopt this value in what follows. This work will be presented in a future paper once the integrations are complete.

N_{JFC}: The total number of observed active Jupiter-family comets with perihelia less than $2.5\,AU$ is approximately 150. Levison & Duncan (1994) found that approximately 10% of comets are active and they spend approximately 7% of their time with perihelia less than $2.5\,AU$. Thus, $N_{JFC} = 21,000$.

r_{Nx}: It is possible to estimate crudely r_{Nx} from our 4 billion year integration presented in Section 2. The largest uncertainty in this calculation is the initial and current distribution of objects within the Kuiper belt. Since neither of these distributions are known, we are forced to make some simple assumptions. We assume that *i*) the initial surface density within the Kuiper belt followed a r^{-2} distribution, *ii*) all the particles in the Kuiper belt had the same initial eccentricity, and *iii*) the only important process that sculpted the Kuiper belt is the gravitational effects of the planets in their current configuration. This model does not take into account the effects of dissipation, collisions, or the possible early migration of the planets. The assumed surface density distribution is consistent with an extrapolation of the distribution of non-volatiles in the outer solar system (see Tremaine 1990). Since the distribution of eccentricities within the Kuiper belt is perhaps the least well constrained parameter, in what follows we adopt two representative values, $e = 0.05$ and 0.15.

To estimate r_{Nx}, we used Monte Carlo techniques to generate an initial population of particles within the Kuiper belt that followed the surface density distribution described above. We then used the results of our simulations in Section 2 to determine the current orbital elements of those particles that were stable for the age of the solar system. In addition, we calculated the number, ΔN, of objects that exited the system in the last 2 billion years. We assumed that r_{Nx} is simply ΔN divided by the product of the total number of particles at the end of the simulation and 2 billion years. We found for objects within $50\,AU$, that $r_{Nx} = 3 \times 10^{-11}$ for the $e = 0.05$ and 5×10^{-11} for $e = 0.15$ models.

We can now estimate the total number of comets in the Kuiper belt interior to $50\,AU$ using Equation (1). For $e = 0.05$ we find that $N_{KB} = 6 \times 10^9$ and for $e = 0.15$ we find that $N_{KB} = 3 \times 10^9$.

By combining this estimate of the number of comets in the Kuiper belt and the Monte Carlo models described above, we can produce models of the current surface number density in the Kuiper belt. The overall result is shown in Figure 8, which gives the radial distribution of comets in the Kuiper belt after 4 billion years for the two different assumed eccentricities. Recall that these models assume that the only important process that sculpted the Kuiper belt is the gravitational effects of the planets in their current configuration. They do not take into account the effects of dissipation, collisions, or the possible early migration of the planets. Both models predict that the trans-Neptunian region is largely depleted at $r \lesssim 36\,AU$. However, if there is a significant number of objects in the 2:3 resonance with eccentricities exceeding ~ 0.15, as appears to be the case in the real Kuiper belt (Marsden 1994, Cochran et al. 1995), we would expect to find objects further in. The peaks seen at $34\,AU$ in the models shown in Figure 8 are due to objects in the mean motion resonances (the 4:5 in the $e = 0.05$ case and the 2:3 in $e = 0.15$ case) seen at perihelion. Thus these peaks are an artifact of the narrow range of eccentricity in each model. In a more realistic model, we might expect to see a plateau in the distribution inside of about $36\,AU$.

High eccentricity objects, which are clearly present in the inner regions of the Kuiper belt, are not included in the models presented above. Therefore, it is not appropriate to compare these models directly with the observations, particularly when observation biases would tend to favor the discovery of high eccentricity objects near perihelion. A more detailed study which includes both observational biases and a more realistic Kuiper belt model is beyond the scope of this paper, but is currently being performed. Nonetheless, we expect many of the main features of the models presented here to persist in more detailed studies.

5. CONCLUSIONS

In this paper we presented the results of a survey of the dynamical behavior of objects in the Kuiper belt. We have performed 2 sets of numerical integrations. In the first we followed the orbital evolution of 1300 test particles on initial orbits of low to moderate eccentricity and *low* inclination within the Kuiper belt, over a period of 4 billion years. In the second we followed the evolution of 3000 particles with initially low to moderate eccentricity and *moderate to high* inclinations within the Kuiper belt for a period of a billion years. These calculations represent the most comprehensive study of the dynamics of objects in the Kuiper belt to date, not only because of the number of particles studied, but also due to the length of time of the integrations.

Our results suggest that the Kuiper Belt has undergone considerable dynamical sculpting largely due to mean motion and secular resonances – a sculpting which is still ongoing. The resulting structure of the belt should to some extent reflect this, in the same sense that much of the structure of the asteroid belt reflects its dynamical evolution under the influence of planetary perturbations (Duncan 1995).

The main results of our investigations are:

1) Resonances cause much of the structure. Overlapping secular resonances induce instabilities in large regions interior to 42 AU, especially at inclinations $\lesssim 25°$. Low order mean motion resonances provide a stabilizing protection mechanism at $i \lesssim 25°$, but are destabilizing at higher inclinations.

2) The Kuiper belt is a plausible source of the progenitors of Jupiter family comets. We have found many regions of the Kuiper belt in which the timescale for instability is on the order of the age of the solar system. These regions include the boundaries of the long-lived mean motion resonances. Thus, for any reasonable orbital element distribution, the long-term erosion of particles is gradual and therefore must be continuing at the current epoch.

3) There is a region ($36\,AU \lesssim a \lesssim\ \sim 39\,AU$ with $i \lesssim 15°$ and $e \lesssim 0.05$) which is dynamically stable for the age of the solar system. The observations to date indicate that this region is unpopulated. If this result is confirmed by further observations, then some mechanism other than the long-term gravitational effects of the planets in their current configuration must have cleared it. This result may provide important and exciting clues to the formation and early evolution of the outer solar system.

4) We have combined the results of the simulations in this paper with our other work on the dynamical evolution of comets interior to Neptune to construct an approximate model for the density distribution in the Kuiper belt. This model does not take into account the effects of dissipation, collisions, or the possible early migration of the planets. From it, we estimate that the total number of comets in the Kuiper belt interior to 50 AU is roughly 5×10^9.

We would like to thank M. Holman, M. Moons, A. Morbidelli, P. Saha, A. Stern, S. Tremaine and P. Weissman for useful discussions. We are also grateful to B. Marsden for providing data and much useful advice. HFL gratefully acknowledges grants provided by the NASA Origins of Solar Systems and Planetary Geology and Geophysics Programs. MJD is grateful for the continuing financial support of the Natural Science and Engineering Research Council and for financial support for work done in the U.S. from NASA Planetary Geology and

Geophysics Programs. We also gratefully acknowledge funding for our computer equipment from the National Science Foundation and the Southwest Research Institute.

REFERENCES

Cochran, A., Levison, H., Stern, S.A, Duncan, M. 1995. Submitted to *Ap. J. Lett.*

Duncan, M. 1995. To appear in *Proceedings of the* 10^{th} *IAP Annual Meeting*

Duncan, M., Quinn, T., & Tremaine, S. 1988. *ApJ*, 328, L69

Edgeworth, K.E. 1949. MNRAS, 109, 600

Everhart, E. 1972. *ApJ*, 10, L131

Everhart, E. 1977. in *Comets–Asteroids–Meteorites,* ed. A.H. Delsemme, (Ohio: University of Toledo Press), 99

Fernández, J. A. 1980. *MNRAS*, 192, 481

Gladman, B., Duncan, M. J. 1990. *Astron. J.* , 100, 1669

Holman, M., & Wisdom, J. 1993. *Astron. J.*, 105, 1987

Jewitt, D., Luu, J. 1995. *Astron. J.*, 109, 1867

Knežević, Z., Milani, A., Farinella, P., Froeschle, Ch., Froeschle, Cl. 1991. *Icarus*, 93, 316

Kozai, Y. 1962. *Astron. J.*, 67, 591

Kuiper, G. P. 1951. In *Astrophysics: A Topical Symposium*, ed. J.A. Hynek, (New York: McGraw Hill), 357

Levison, H., & Duncan, M. 1993. *Ap. J.* , 406, L35

Levison, H., & Duncan, M. 1994. *Icarus*, 108, 18

Levison, H., & Stern, S.A. 1995. To appear in *Icarus*

Malhotra, R. 1993. *Nature*, 365, 819

Malhotra, R. 1995. To appear in *Astron. J.*

Marsden, B. 1994. IAU Circular No. 5984

Morbidelli, A., Thomas, F., & Moons, M. 1995. Submitted to *Icarus*

Newton, H. A. 1893, *Mem. Nat. Acad. Washington*, 6, 7

Quinn, T., Tremaine, S., & Duncan, M., 1990. *ApJ*, 355, 667

Saha, P., and Tremaine, S. 1993, *Astron. J.*, 104, 1633

Stern, S.A. 1991. *Icarus*, 90, 271

Stern, S.A. 1995. To appear in *Astron. J.*

Thomas, F., & Morbidelli, A. 1995. Preprint

Torbett, M. 1989. *Astron. J.*, 98, 1477

Torbett, M., Smoluchowski, R. 1990. *Nature*, 345, 49

Tremaine, S. 1990, in *Baryonic Dark Matter,* ed. D. Lynden-Bell and G. Gilmore, (Kluwer, Dordrecht), 37

Wetherill, G. W. 1991. *Science*, 253, 535

Wisdom, J., & Holman, M. 1991. *Astron. J.*, 102, 1528

Table 1
Marsden's Orbital Elements of the Known Kuiper Belt Objects

Name	a (AU)	Resonance	e	i (Deg)	ω (Deg)	Ω (Deg)	M (Deg)	Status
1992 QB1	43.94	–	0.070	2.2	359	0	6	MPC 24408
1993 FW	43.86	–	0.052	7.7	43	188	323	MPC 25227
1993 RO	39.34	2:3	0.120	3.7	187	170	357	MPC 25241
1993 RP†	39.42	2:3	0.116	2.6	180	192	3	MPC 23493
1993 SB	39.45	2:3	0.324	1.9	79	355	319	Stable
	39.39	2:3	0.322	1.9	79	355	320	MPC 24408
	36.30	3:4	0.182	1.9	68	355	315	Unstable
	42.16	3:5	0.399	1.9	82	355	325	Unstable
1993 SC	39.47	2:3	0.180	5.2	319	355	34	MPC 24763
1994 ES2	45.93	–	0.125	1.0	100	155	279	MPC 24900
1994 EV3	43.07	–	0.038	1.7	14	20	165	MPC 25228
1994 GV9	43.73	–	0.042	0.6	335	177	21	MPC 25228
1994 JS	42.52	3:5	0.186	14.0	140	56	29	MPC 25218
	42.48	3:5	0.184	14.0	140	56	29	Stable
	42.14	3:5	0.165	14.0	148	56	24	Unstable
1994 JQ1	44.19	–	0.027	3.7	211	26	335	MPC 25228
1994 JR1	39.71	2:3	0.125	3.8	99	145	1	MPC 25228
	39.89	2:3	0.131	3.8	87	145	11	Unstable
1994 TB†	39.61	2:3	0.375	12.2	317	318	39	Unstable
	39.57	2:3	0.292	12.0	340	317	31	MPC 25124
	36.47	3:4	0.171	12.0	73	317	333	Stable
	36.55	3:4	0.154	12.0	55	317	346	Stable
1995 DA2†	36.34	3:4	0.116	6.6	62	127	309	MPC 25184
	36.34	3:4	0.061	6.2	0	127	0	Stable
	47.90	2:1	0.309	5.3	0	127	0	Unstable
	47.42	2:1	0.302	5.3	0	127	0	Unstable
	47.30	2:1	0.300	5.4	0	127	0	Unstable
	34.78	4:5	0.012	6.4	0	127	0	Unstable
	42.14	3:5	0.204	5.7	0	127	0	Stable
1995 DB2†	43.49	–	0.067	4.3	0	129	0	MPC 25184
1995 GJ†	42.91	–	0.091	22.9	180	339	0	MPC 25185
1995 GA7†	39.46	2:3	0.119	3.5	100	21	64	MPC 25186

† The orbits for these objects are not well known because the observed arcs very small. Planetary perturbations were not considered in the computation of the orbit.

FIGURE CAPTIONS

Figure 1 — The crossing time for particles in the Kuiper belt derived from our first set of calculations (initial $i = 1°$, duration of $4\,Gyr$). Each particle is represented by a narrow vertical strip of color, the center of which is located at the particle's initial eccentricity and semi-major axis. The color of each strip represents the dynamical lifetime of the particle as defined in the text. Strips that are colored yellow represent objects that survive for the length of the integration, 4 billion years. Dark regions are particularly unstable on these timescales. The colored circles represent the the location of possible orbits for the known Kuiper belt objects as determined by Brian Marsden. The filled green circles implies that the orbit is considered the the current best orbit for this object. The open green and red circles represent the other stable and unstable orbits, respectively. The filled blue circles show the current heliocentric distances of the 7 Kuiper belt objects for which only circular orbits have been computed. For reference, the locations of the important Neptune mean motion resonances are shown in blue and two curves of constant perihelion distance, q, are shown in red. The small blue double-headed arrow shows the width of the 3:2 resonance at the location of Pluto's orbit (Levison & Stern 1995).

Figure 2 — Similar to Figure 1 except for the second set of calculations. In this case the length of the integration was 1 billion years. Each particle is represented by a narrow vertical strip of color, the center of which is located at the particle's initial inclination and semi-major axis. The color of each strip represents the dynamical lifetime of the particle as defined in the text. The three different panels show data for objects with three different eccentricities, $0.01, 0.05, 0.1$.

Figure 3 — An enlargement of the bottom panel of Figure 2 with the secular and mean motion resonances plotted. Note that we used a different color table to produce this plot. The red curve and yellow curves show the locations of Neptunian longitude of perihelion secular resonances (ν_8) and the Neptunian longitude of the ascending node secular resonances (ν_{18}), respectively, as determined by Knežević *et at.* (1991). The green lines show the location of the important Neptune mean motion resonances.

Figure 4 — The temporal behavior of a particle near the 3:4 mean motion resonance ($a = 36.5\,AU$) with initial $i = 45°$ and $e = 0.01$. This particle is stopped because it encounters Uranus. A) The critical argument of the ν_8 resonance. At early times it appears that the particle was librating about the ν_8 resonance. B) The critical argument of the Neptune 3:4 mean motion

resonance. The particle appears to librate about this resonances at late times. C) The eccentricity.

Figure 5 — The dynamical lifetimes of particles in the 3:2 mean motion resonances with Neptune as a function of initial libration amplitudes, A_δ. All these particles had initial $e = 0.2$ and $i = 1°$. The dotted line indicates the length of the integration, 4 billion years. Thus, symbols on this line represent objects that survived the entire integration. It is important to note that there were particles that were stable for billions of years and yet became unstable before the end of the integration.

Figure 6 — The temporal behavior of a particle initially in the 3:4 mean motion resonance ($a = 36.5\,AU$) with initial $i = 1°$ and $e = 0.15$. This object is one that remained stable for billions of years and then became unstable at the very end of the integration. A) The inclination. Note that the inclination remains small until near the end of the integration, then it was pumped up to 20°. B) The perihelion distance. C) The 3:4 libration amplitude. Note that the object was in the resonance while it was stable, sometimes having a very small libration amplitude.

Figure 7 — The inclinations of objects leaving the Kuiper belt between 1 and 4 billion years as a function of their initial semi-major axes. All these particles had initial $i = 1°$. Different symbols refer to the initial eccentricity of the particles. The important mean motion resonances are also shown.

Figure 8 — The current surface density distribution of comets in the Kuiper belt as determined by our Monte Carlo simulation. These models assume that the distribution initially follows a power law with an exponent of -2 (shown as a dotted curve) and that all comets had the same initial inclination $i = 1°$ and eccentricity, e. A) $e = 0.05$. B)$e = 0.15$.

FIGURE 1

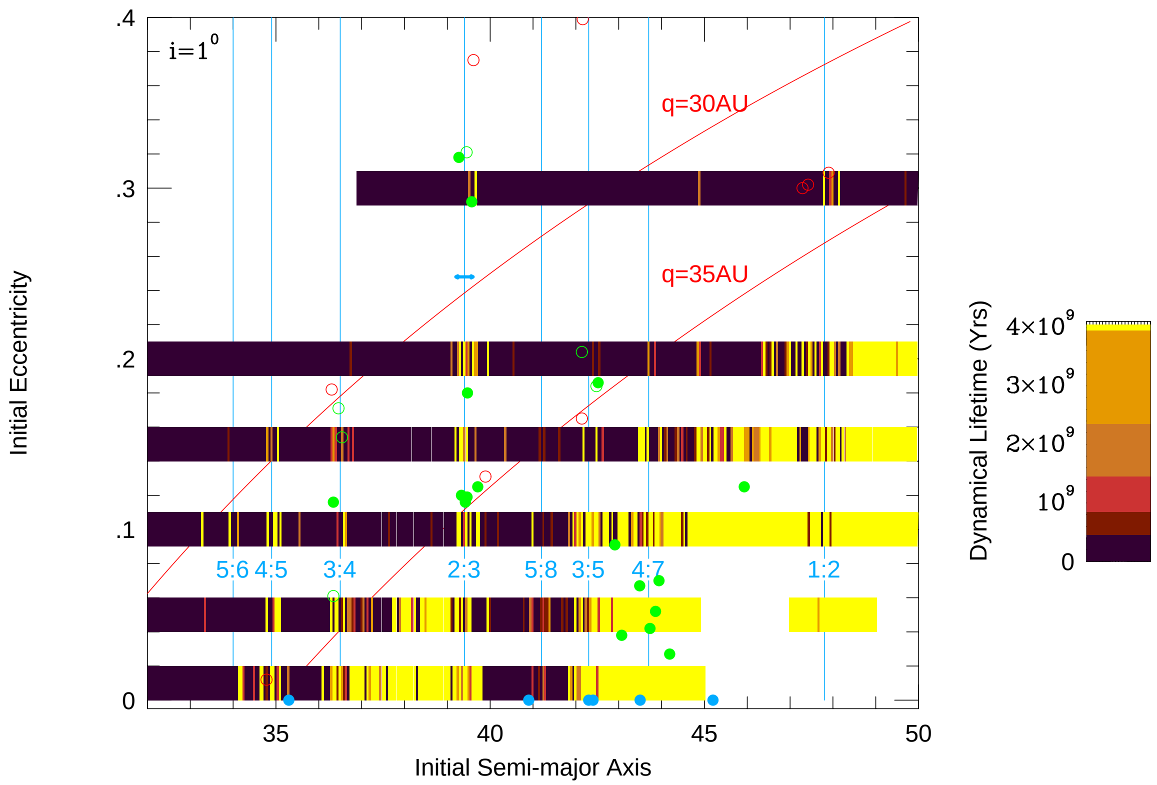

i=1°
q=30AU
q=35AU
5:6 4:5
3:4
2:3
5:8
3:5
4:7
1:2
.4
.3
.2
.1
0
35
40
45
50
Initial Eccentricity
Initial Semi-major Axis
Dynamical Lifetime (Yrs)
4×10⁹
3×10⁹
2×10⁹
10⁹
0

FIGURE 2

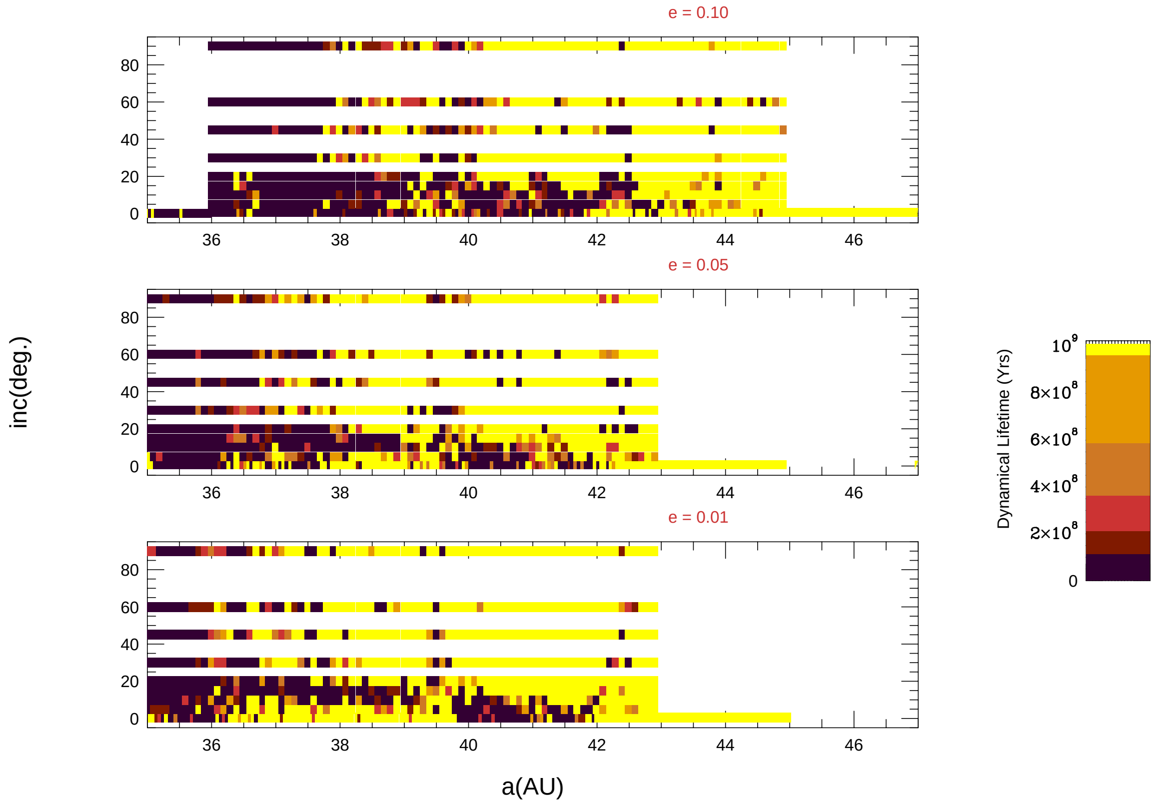
e = 0.10
e = 0.05
e = 0.01
inc(deg.)
a(AU)
Dynamical Lifetime (Yrs)
10^9
8×10^8
6×10^8
4×10^8
2×10^8
0
80
60
40
20
0
36
38
40
42
44
46

FIGURE 3

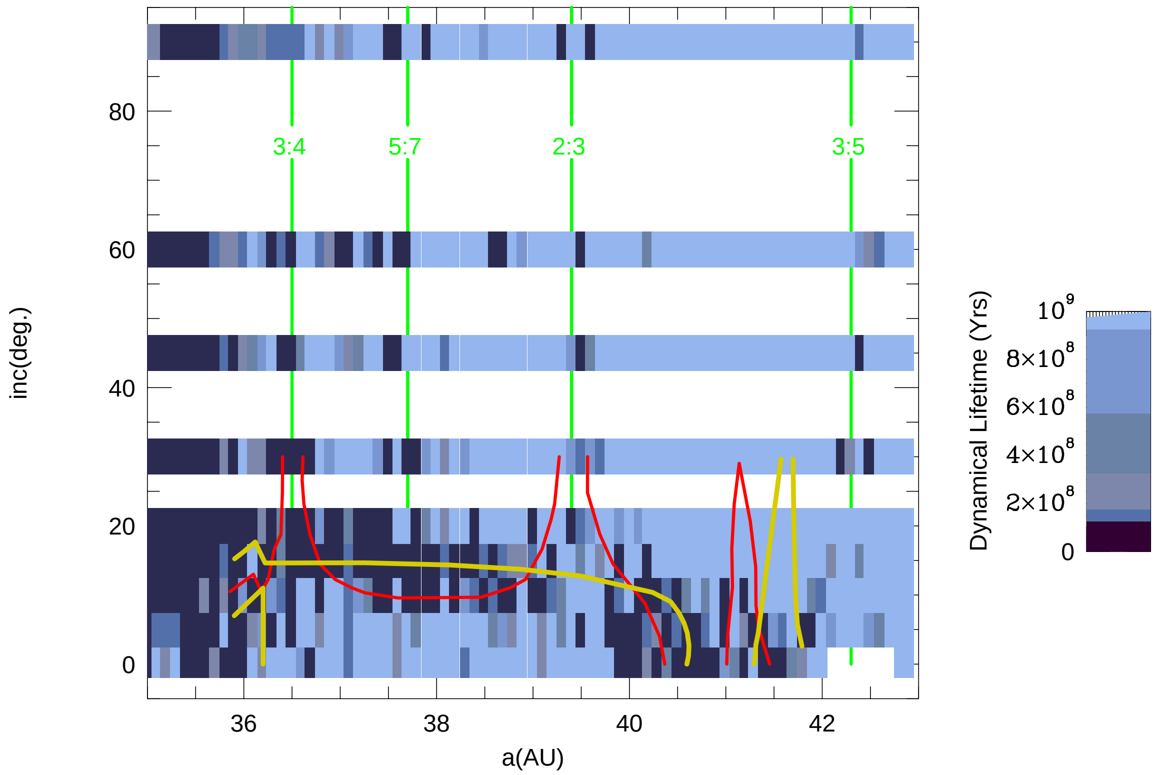

3:4
5:7
2:3
3:5
80
60
40
20
0
inc(deg.)
36
38
40
42
a(AU)
Dynamical Lifetime (Yrs)
10^9
8×10^8
6×10^8
4×10^8
2×10^8
0

FIGURE 4

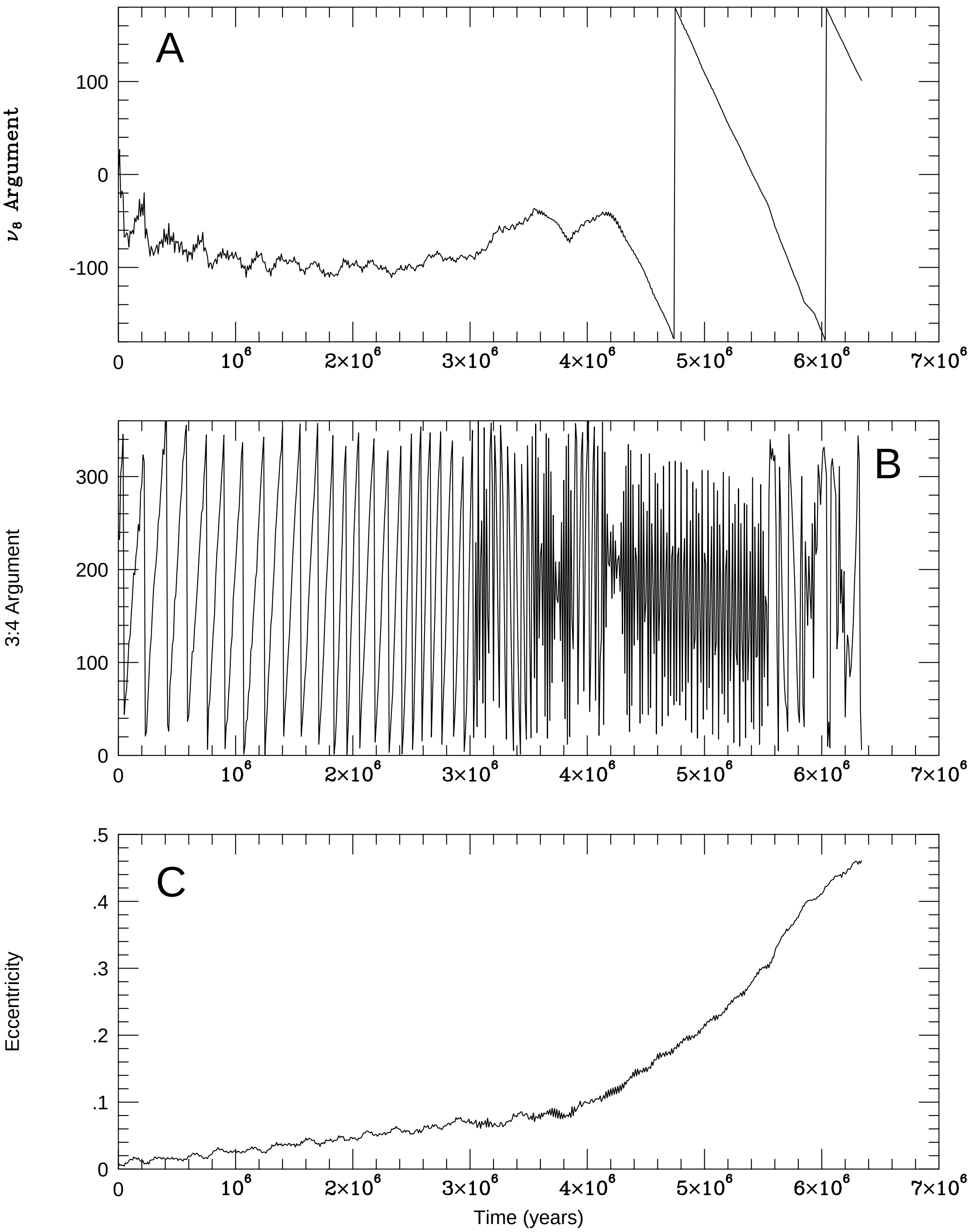
A
100
0
-100
ν_8 Argument
0
10^6
2×10^6
3×10^6
4×10^6
5×10^6
6×10^6
7×10^6
B
300
200
100
0
3:4 Argument
0
10^6
2×10^6
3×10^6
4×10^6
5×10^6
6×10^6
7×10^6
C
.5
.4
.3
.2
.1
0
Eccentricity
0
10^6
2×10^6
3×10^6
4×10^6
5×10^6
6×10^6
7×10^6
Time (years)

FIGURE 5

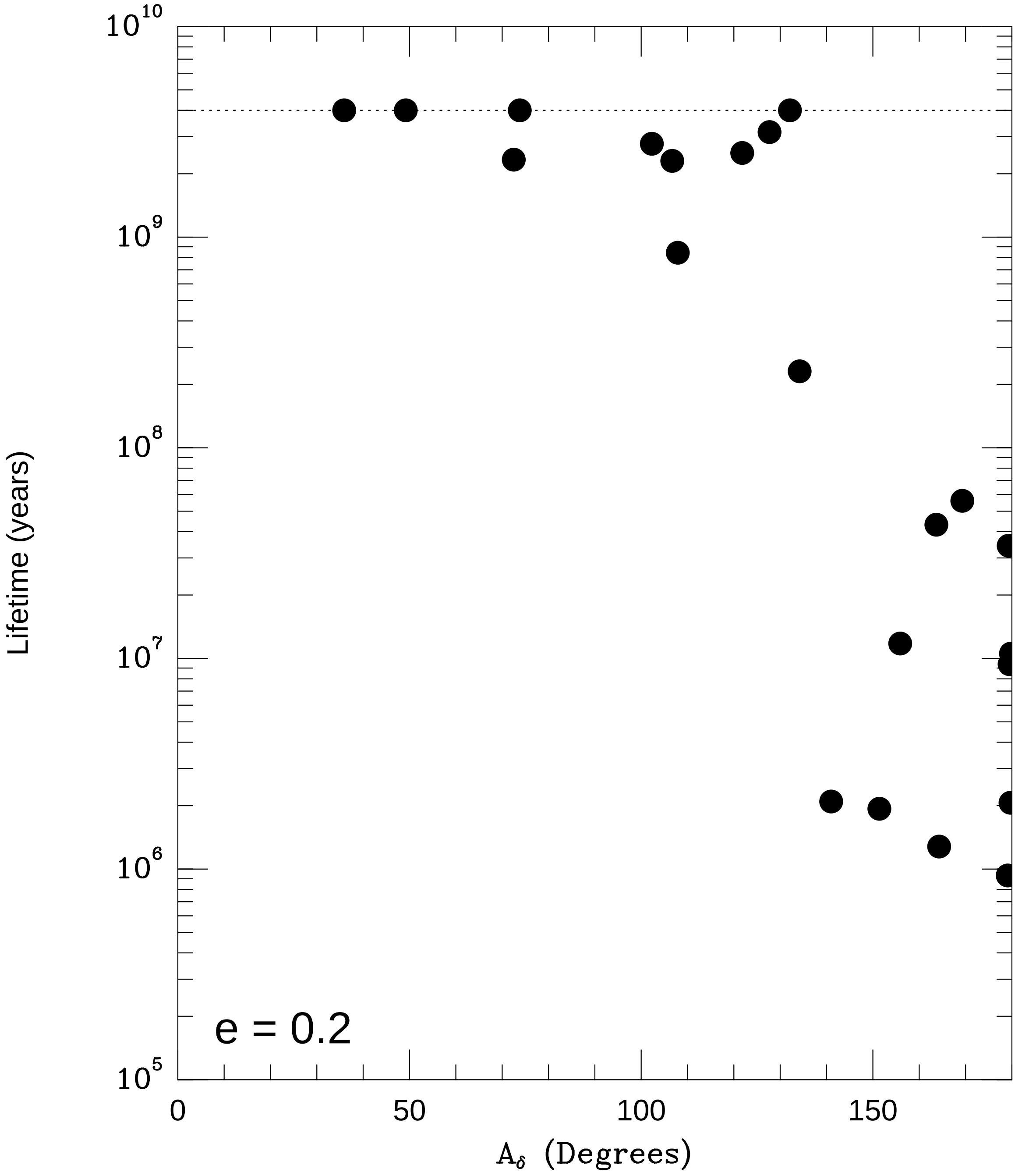

10^{10}
10^{9}
10^{8}
10^{7}
10^{6}
10^{5}
Lifetime (years)
e = 0.2
0
50
100
150
A_δ (Degrees)

FIGURE 6

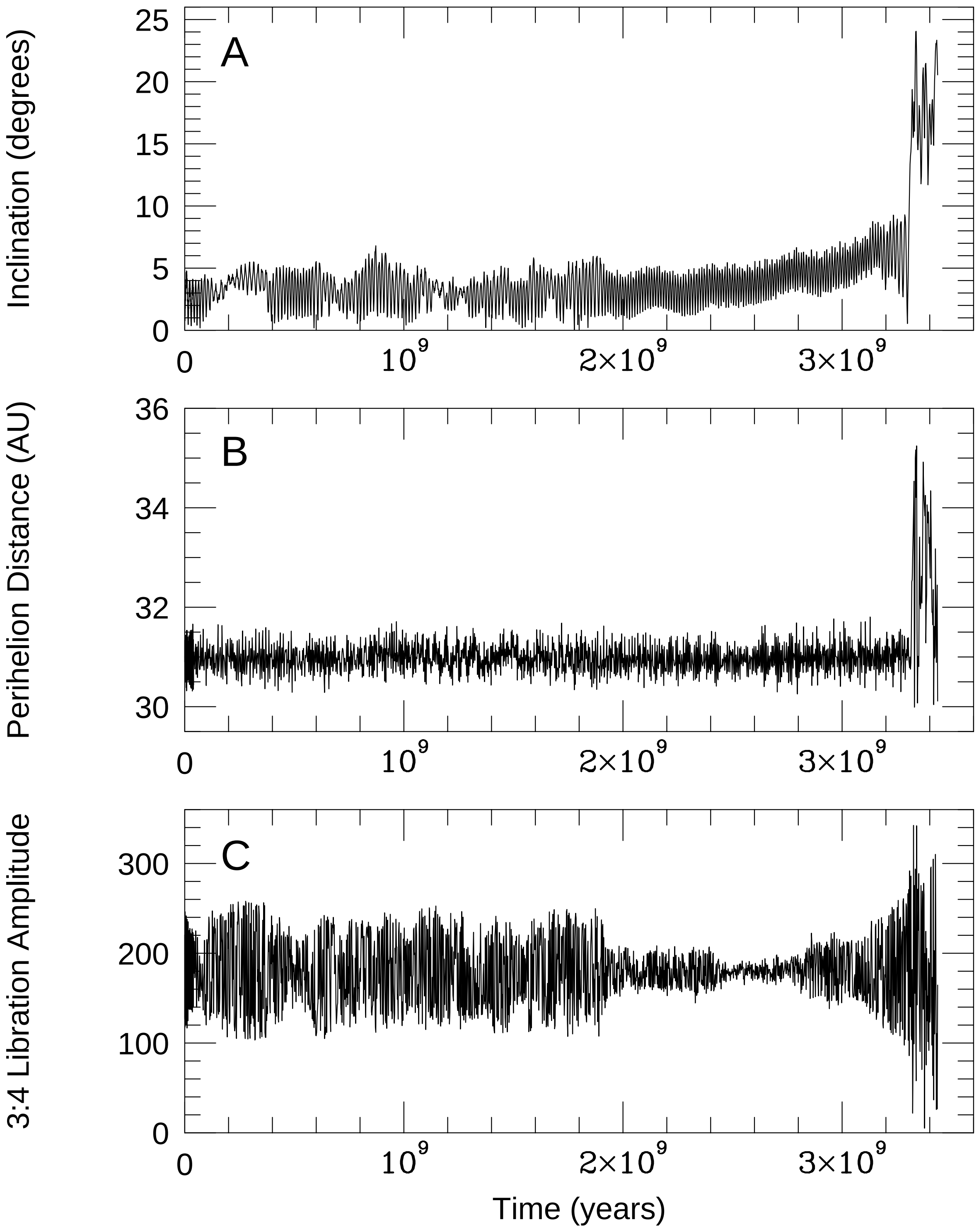
A
B
C
Inclination (degrees)
Perihelion Distance (AU)
3:4 Libration Amplitude
Time (years)
0
5
10
15
20
25
30
32
34
36
100
200
300
10^9
2×10^9
3×10^9

FIGURE 7

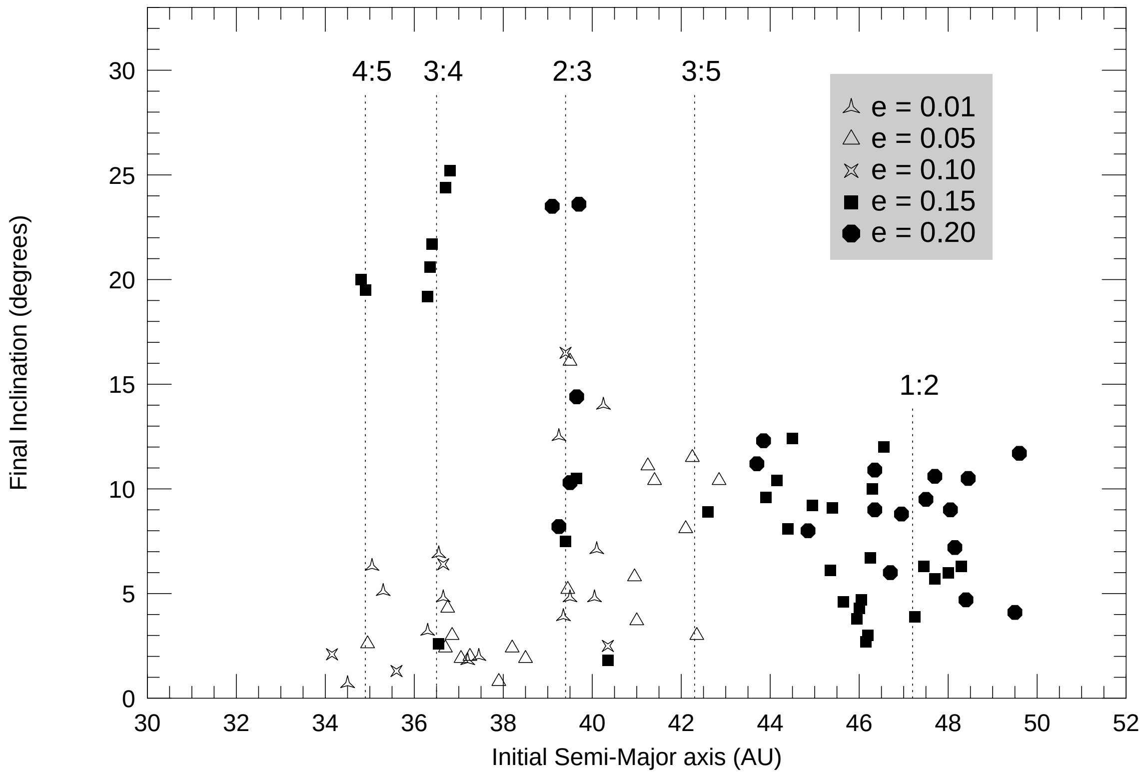

4:5
3:4
2:3
3:5
1:2
e = 0.01
e = 0.05
e = 0.10
e = 0.15
e = 0.20
Final Inclination (degrees)
Initial Semi-Major axis (AU)
0
5
10
15
20
25
30
30
32
34
36
38
40
42
44
46
48
50
52

FIGURE 8

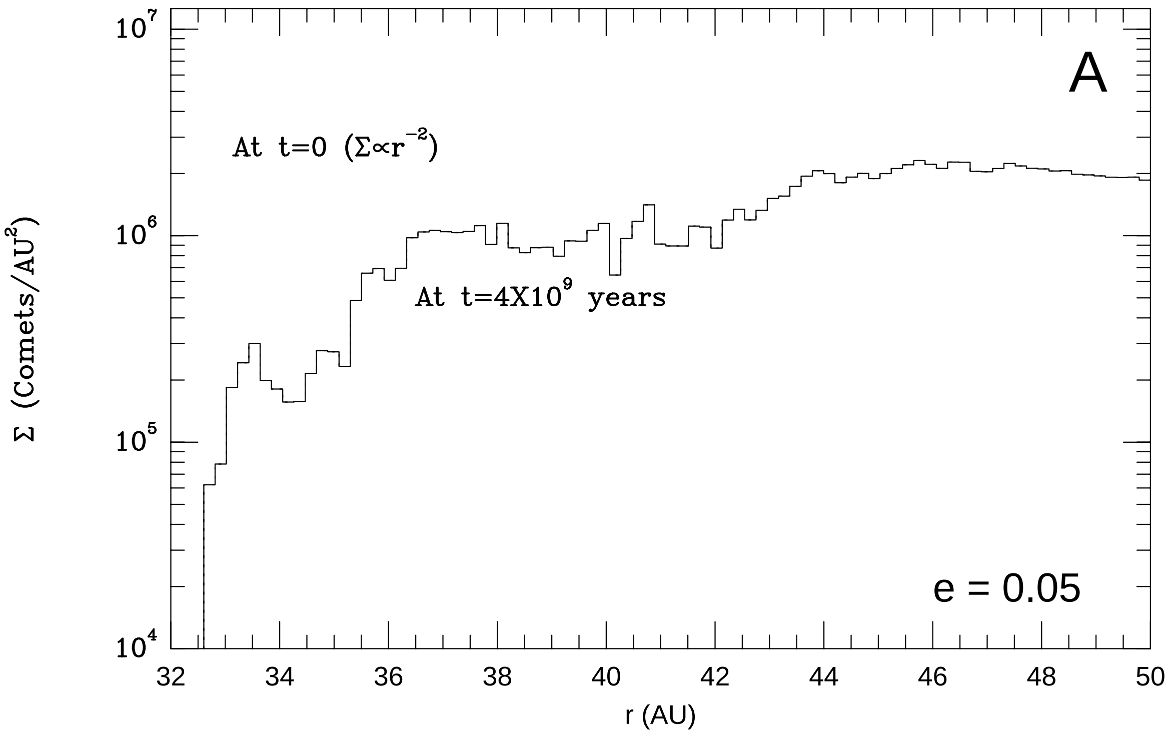

A
At t=0 (Σ∝r^{-2})
At t=4X10^{9} years
e = 0.05
Σ (Comets/AU^{2})
r (AU)
10^{4}
10^{5}
10^{6}
10^{7}
32
34
36
38
40
42
44
46
48
50

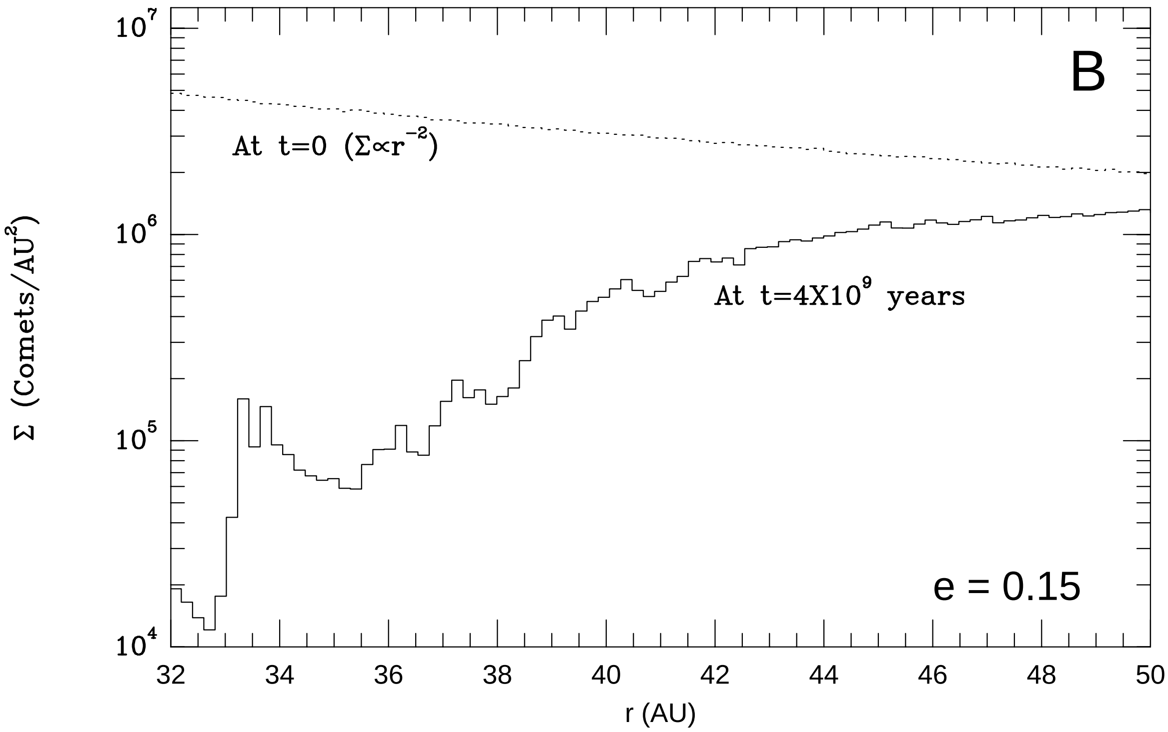

B
At t=0 (Σ∝r^{-2})
At t=4X10^{9} years
e = 0.15
Σ (Comets/AU^{2})
r (AU)
10^{4}
10^{5}
10^{6}
10^{7}
32
34
36
38
40
42
44
46
48
50